ADVANCED MATERIALS
www.advmat.de

3D Lifetime Tomography Reveals How $CdCl_2$ Improves Recombination Throughout CdTe Solar Cells

Edward S. Barnard, Benedikt Ursprung, Eric Colegrove, Helio R. Moutinho, Nicholas J. Borys, Brian E. Hardin, Craig H. Peters, Wyatt K. Metzger, and P. James Schuck**

Composition and structural inhomogeneities are hallmark characteristics of novel electro-optic materials and can substantially influence overall device performance. For next-generation solar-cell technologies, accurately measuring and untangling bulk, interface, and grain-boundary carrier recombination persists as one of the single greatest challenges in understanding these materials and expanding their applications. This challenge is especially relevant in polycrystalline thin films of direct-bandgap semiconductors. These materials enable the fabrication of both ridged and flexible optoelectronic devices where the photoactive medium is just a few micrometers thick. Rapid deposition of such films with low capital equipment costs can revolutionize electronics and create the next generation of ultralow cost, high-performance solar technology. For example, CdTe, $Cu(In,Ga)Se_2$, and perovskite solar cells have recently exceeded or matched the record solar-cell efficiency of the dominant technology, multicrystalline-Si (mc-Si).[1] CdTe is particularly attractive because it is currently manufactured at costs less than those of mc-Si, yet produces solar cells with similar efficiencies.[2] Substantial improvements to carrier lifetime can still further enhance the efficiency, thereby enabling CdTe and other thin-film technologies to provide electricity at costs less than conventional energy sources.

Because CdTe films, like the majority of polycrystalline films, are rapidly deposited, the crystalline grain sizes are commensurate with the film thickness, which is typically just several micrometers. In addition, *p–n* junctions are formed by deposition on top of a layer that is often lattice mismatched, producing a highly defective interface.[3,4] As a result, adverse nonradiative carrier recombination at this interface, at grain boundaries, and in the inhomogeneous bulk critically shape aggregate carrier lifetime and impact performance. However, there has been a lack of measurements quantifying and discriminating between grain-boundary, interface, and bulk recombination in these semiconductor materials. Not having this information impedes both the identification of the key recombination mechanisms and the monitoring of how processing affects such carrier dynamics, forcing empiricism, and conjecture in lieu of scientific results. While PL intensity mapping can provide some information, it is ultimately limited as the recorded signal is an intricate convolution of carrier concentration, external and internal optical transmission, and recombination, so the results do not directly correspond to recombination. Here, we determine carrier lifetimes by counting single photons emitted as a function of time after two photons from fast laser pulses excite carriers in targeted semiconductor regions. With this 3D two-photon lifetime tomography, we extract and map carrier lifetimes, a direct metric for recombination dynamics, throughout the entirety of a CdTe photovoltaic active material with unprecedented access to the bulk and buried subsurface structures.

In CdTe solar cells, a $CdCl_2$ treatment step is universally used to significantly improve device performance.[5,6] This treatment is known to induce two changes in the CdTe active layer: i) recrystallization and grain coalescence of the CdTe film[7,8] and ii) preferential Cl concentration at the grain boundaries that has been hypothesized to passivate the local nonradiative recombination.[9–12] The perceived effects on carrier dynamics at grain boundaries have been derived from enhanced signals in electron-beam-induced current (EBIC) studies.[9,13,14] However, defective grain boundaries can produce small potentials that attract minority carriers, thereby increasing the EBIC signal, the photocurrent, and dark current, but decreasing open-circuit voltage and efficiency,[15] leaving conclusions about the treatment's role ambiguous. Previous one-photon PL mapping has proven crucial in illuminating defect-related recombination mechanisms[16] in near-surface material. But for film thicknesses comparable to or thicker than optical absorption lengths (e.g., ≈100 nm in CdTe), one-photon measurements are dominated by surface recombination and therefore exhibit extrapolated bulk carrier lifetimes that deviate strikingly (>10×) from the actual values as determined recently by multiphoton excitation.[17] Notably, direct lifetime measurements throughout the polycrystalline device elucidating subsurface grain boundary recombination have not yet been shown. In this work, 3D lifetime tomography reveals that the $CdCl_2$ treatment not only improves carrier lifetimes throughout the film, but also strongly improves carrier lifetime at grain boundaries and interfaces—including the surface and the p–n junction—leaving the film with a much longer local aggregate carrier-lifetime distribution.

Dr. E. S. Barnard, Dr. N. J. Borys, Dr. P. J. Schuck
Molecular Foundry
Lawrence Berkeley National Laboratory
Berkeley, CA 94720, USA
E-mail: esbarnard@lbl.gov; pjschuck@lbl.gov
Dr. E. S. Barnard, B. Ursprung, Dr. B. E. Hardin, Dr. C. H. Peters
PLANT PV, Inc.
Alameda, CA 94501, USA
Dr. E. Colegrove, Dr. H. R. Moutinho, Dr. W. K. Metzger
National Renewable Energy Laboratory
Golden, CO 80401, USA

DOI: 10.1002/adma.201603801

ADVANCED MATERIALS
www.advmat.de

www.MaterialsViews.com

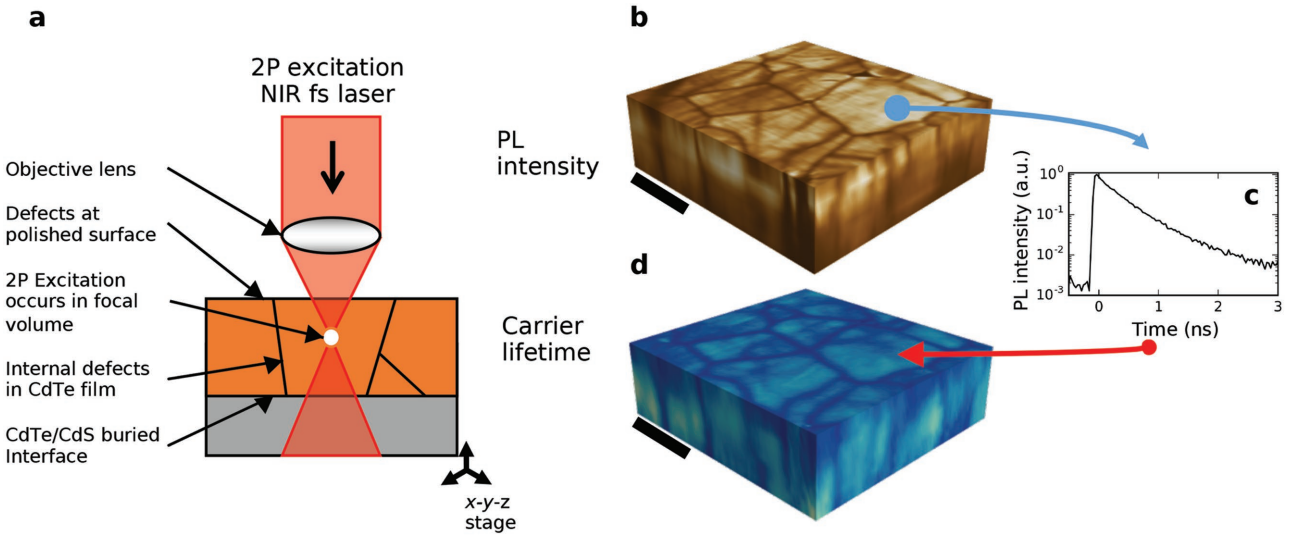

Figure 1. 3D 2P-TRPL microscopy of CdTe thin films. a) Schematic of 2P-TRPL microscopy measurements. b) A representative 3D data cube of PL intensity data acquired with 2P-TRPL microscopy. (c) At each data point we acquire a lifetime trace and extract a representative lifetime, as described in the text, to form d) a 3D lifetime data cube. Scale bars are 10 µm.

These results demonstrate the importance of directly imaging changes in recombination at key subsurface structures such as grain boundaries and buried interfaces.

Two-photon absorption measurements use photons with energies below the bandgap to excite semiconductor charge carriers via nonlinear optical absorption. While heavily used in bioimaging,[18] multiphoton microscopy has only seen limited application in materials science.[17,19–21] Efficient multiphoton excitation requires near-simultaneous absorption of multiple photons and exhibits a nonlinear dependence on excitation density. This process can occur at photon energies where a semiconductor is transparent to linear (one-photon) absorption. Therefore, using a confocal microscope, it is possible to confine the excitation to a subsurface diffraction-limited volume. As is shown schematically in **Figure 1**a, we can systematically scan this excitation volume throughout the film to form complete 3D carrier lifetime and photoluminescence (PL) intensity maps. Thus, using two-photon absorption as a carrier excitation source allows the independent examination of grain boundary (GB) and interior (GI) regions at the front surface, bulk, and buried interfaces of thin-film materials and devices.

The 3D maps of carrier lifetime are acquired by rastering the sample under a focused 150 fs pulsed laser beam (Ti:sapphire-pumped Optical Parametric Oscillator) with a repetition rate of 76 MHz and wavelength of 1100 nm. The laser is focused with a microscope objective (100×, 0.95 numerical aperture) to a diffraction-limited spot within the sample and lifetime traces of the two-photon-induced PL emission (Figure 1c) are collected via time-correlated single-photon counting (Picoquant PicoHarp). Photoinduced carrier injection levels are higher than typical carrier concentrations in CdTe, and thus may reduce interface contrast.[22] Reabsorption of PL can occur as photons exit the material from subsurface measurements. Consequently, we observe that the PL spectrum redshifts as the probe position goes deeper into the sample. To mitigate this effect, we use an 840 nm/10 nm band-pass filter to only collect the red side of the emission spectrum, which is minimally affected by reabsorption. This allows us to consistently collect from the same electronic state transition throughout a 3D scan.

Each lifetime trace is collected from the sample with a voxel size comparable to the diffraction-limited focal volume (≈500 nm in diameter, ≈3 µm in depth). While diffusion away from the collection volume and large excited carrier concentration may affect measured decay traces, the principal lifetime variation throughout the film is attributed to recombination.[17] For display and data interpretation, the intensity (Figure 1b) and lifetime (Figure 1d) are extracted from each voxel to create a 3D lifetime data cube (Figure 1d). The lifetime is taken as when $1/e^2$ of photons are left in the integrated time trace. We choose this value because it provides a low noise metric that captures both short and long lifetime components of the multi-exponential data. In parallel, we execute least-squared fitting of the data to monoexponential or biexponential functions; while not shown, the results produce the same trends and conclusions described here.

Carrier recombination and device performance in CdTe solar cells can be critically enhanced by $CdCl_2$ treatment. To understand how $CdCl_2$ affects carriers, we measured samples at different stages in the fabrication process of a standard superstrate CdTe solar cell: i) after CdTe close-space sublimation (CSS) deposition, ii) after $CdCl_2$ treatment, and iii) after device completion. In some samples, the CdTe layer was thicker (≈15 µm) than in typical devices to show lifetime variations throughout the film more clearly. These CdTe layers were grown at 625 °C substrate temperature in an ambient atmosphere of N_2 at a pressure of 10 Torr for 6 min. We also prepared 5 µm thick complete CdTe devices with typical efficiencies of 15%, where the CdTe was deposited by CSS at 600 °C in an ambient of oxygen and helium at 16 Torr for 2 min and 30 s. The $CdCl_2$ treatment was performed at 400 °C for 10 min using a vapor in a CSS chamber. Copper and gold contacts were deposited at room temperature by evaporation and a final annealing step

Adv. Mater. **2016**,
DOI: 10.1002/adma.201603801

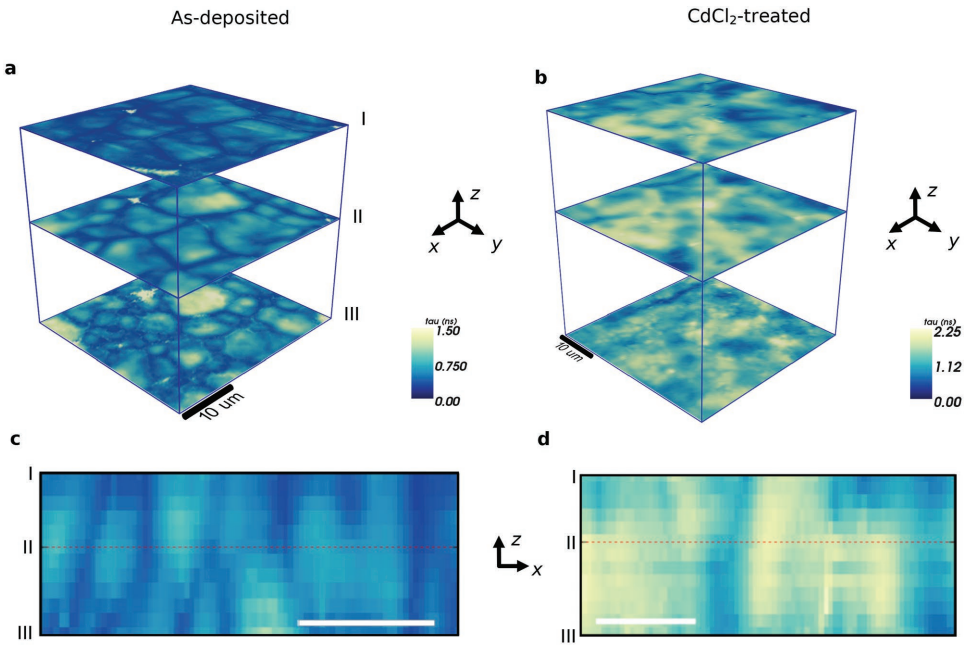

Figure 2. 3D tomographic comparison of carrier lifetimes between as-grown and $CdCl_2$-treated CdTe films. a,b) Horizontal cuts (i.e., planes parallel to the top surface) of the carrier lifetimes at discrete sample depths (I: surface, II: bulk, III: buried CdTe/CdS interface) for the as-deposited sample (a) and the $CdCl_2$-treated sample (b). c,d) Representative depth cross-sections (i.e., orthogonal to the top surface) of carrier lifetimes for the as-deposited sample (c) and $CdCl_2$-treated sample (d). All scale bars are 10 µm.

was performed at 211 °C for 30 min in a tube furnace under flowing helium. In some samples, a back contact was not added so as to maintain optical access. These thick samples were mechanically polished to flatten as-grown surface roughness and reduce optical scattering.

Figure 2 shows representative slices of the 3D maps of carrier lifetime for polished samples before and after a $CdCl_2$ treatment. Figure 2a,b show lateral (x–y) slices from one of the 3D data sets at representative depths in the samples: I) polished top surface of the CdTe layer; II) the bulk of the CdTe layer (5 µm below the surface); and III) the CdTe/CdS p–n heterojunction interface. The first observation from these maps is the dark lines in the as-deposited map (left). These correspond to grain boundaries in the untreated sample where local carrier lifetime is reduced significantly compared with neighboring areas. Correlated electron back-scatter diffraction (EBSD) measurements (see **Figure 3**) confirm that these contours of reduced lifetime directly correspond to CdTe grain boundaries. Unlike the as-deposited sample, the $CdCl_2$-treated sample (right) shows a significantly more homogeneous lifetime distribution, making grain boundaries nearly unresolvable in the lifetime tomography data. For clarity, we present here only one set of tomographic data from each sample, though we note that we have performed 3D lifetime scans over multiple spatially separated areas on each of these samples as well as on additional samples, with comparable results.

The post-treatment reduction in lifetime contrast between grain boundaries and grain interiors extend through the entire thickness of the film. For example, the cross-sectional lifetime distribution of the as-deposited sample in Figure 2c reveals vertical columns of reduced lifetime that correspond to carrier recombination at grain boundaries that span the film thickness. We also note the grain size varies throughout the film with smaller seed grains observed near the CdTe/CdS interface. The p–n junction is located at this interface, so the GB recombination in this region diminishes aggregate lifetime and helps explain why performance of as-deposited CdTe device films is poor. As the films are grown, these small seed grains coalesce to form larger columnar grains away from the interface in the top 5 µm of the film. This can be visualized more strikingly in the movie of this 3D lifetime map that is available in the Supporting Information. Similar grain growth morphology has been observed by others in electron microscopy studies.[23] Remarkably, after the $CdCl_2$ treatment, the deleterious GB recombination throughout the film is reduced as seen in Figure 2d. Most importantly, the lifetime near the CdTe/CdS interface improves substantially after $CdCl_2$ treatment, which is directly quantified and visualized here for the first time.

We use EBSD to help classify each voxel within our scans and to quantify carrier-lifetime differences between the grain interiors (GIs) and grain boundaries (GBs). EBSD measures local crystallographic orientation at the sample surface and allows us to discriminate different grains and spatially map the corresponding GBs. Figure 3a,b show lateral slices of carrier lifetimes near the surface of the as-deposited and $CdCl_2$-treated samples, respectively. Figure 3c,d show EBSD maps of the same regions that are correlated to 2P-TRPL maps using fiducial marks. For the case of the as-deposited sample, lines of reduced lifetimes are clearly correlated with the GBs observed in EBSD, as illustrated by the overlaid red contours in Figure 3a. However, for the $CdCl_2$-treated sample (Figure 3b), a reduced carrier lifetime does not correlate to GB regions and in fact, some of the boundary areas exhibit longer lifetimes than neighboring grains. The direct correlation of lifetime imaging and EBSD

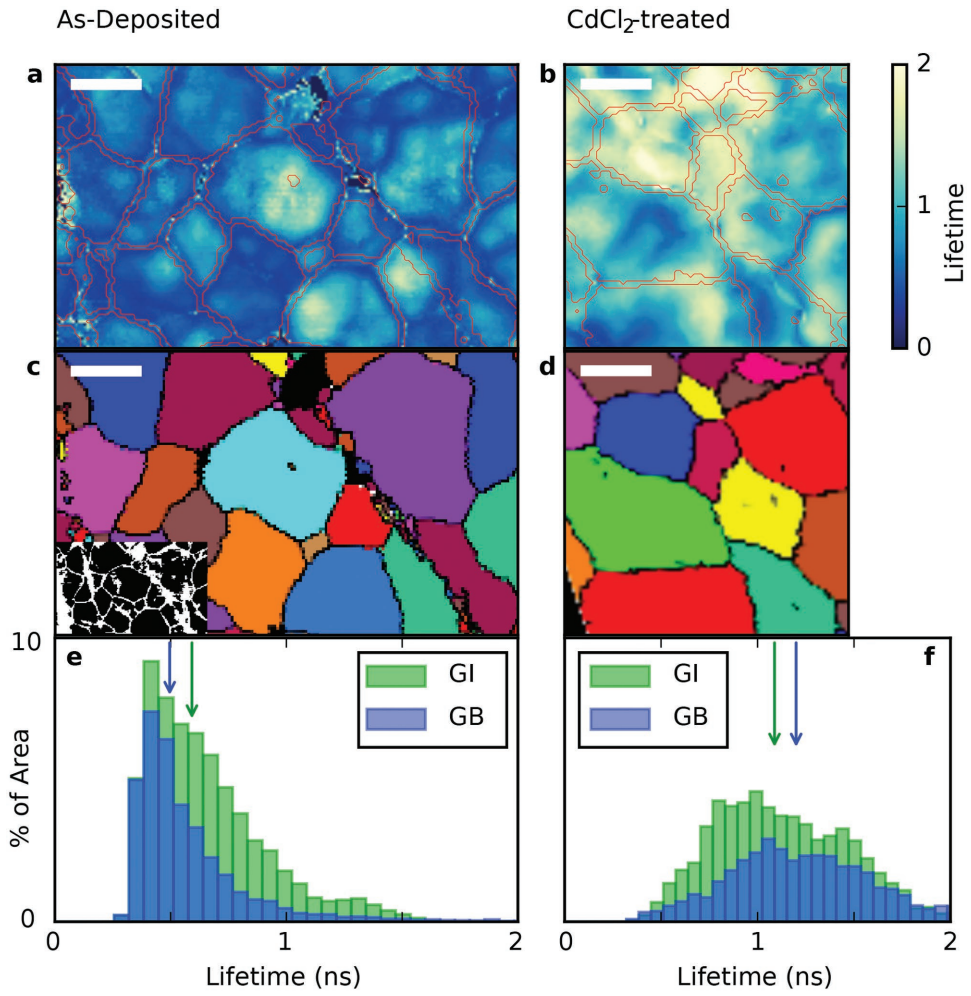

Figure 3. Carrier lifetimes in grains and at grain boundaries in as-deposited and $CdCl_2$-treated CdTe films. a,b) 2P-TRPL maps near the sample surface with overlaid EBSD grain mapping. Scale bars are 10 µm. a) Carrier-lifetime map of the as-deposited sample overlaid with red contours that mark GB regions. b) Similar map of carrier lifetimes in the $CdCl_2$-treated sample. c,d) Corresponding EBSD maps of the regions, showing the locations of grains and GBs. c) Inset shows a slice of PL-intensity threshold map used in full-volume GB/GI separation. Inset is reduced in size by 3×. e,f) Histograms of GI (green) and GB (blue) lifetimes in this near-surface layer for the two samples. The arrows note the median lifetime value for each voxel type (green for GI, blue for GB). e) As-deposited sample. f) $CdCl_2$-treated sample.

allows us to unambiguously associate recombination to GB or GI material. While the GB positions are relatively clear in the as-deposited optical lifetime maps, they are significantly less obvious in PL lifetime maps of the treated samples. Therefore, the EBSD-lifetime tomography correlation proves critical for elucidating the effect of the $CdCl_2$ treatment on the cell.

With the classification of voxels as belonging to GB or GI regions, we can statistically compare the two large sets of individual points. Figure 3e,f statistically catalog the carrier lifetimes for GB and GI regions for the surfaces of the two samples. For the as-deposited sample, GB regions have a median carrier lifetime that is 14% shorter than that of the GI. For the $CdCl_2$ sample, the distributions of both GB and GI lifetimes are shifted to longer decay times, and the median lifetime of the boundaries is now slightly longer than the grain interiors.

In addition to extracting statistics on the lifetime contrast between GIs and GBs near the surface, these 3D lifetime maps allow us to understand variations in carrier lifetime throughout the depth of the film. For the case of the as-deposited sample, classifying voxels as belonging to either a GB or GI based on their PL intensity allows us to explore trends in carrier lifetime throughout the film depth at grain boundaries and interiors. **Figure 4**a shows this 3D map of the separation of GI and GB voxels as determined by a PL intensity threshold for the as-deposited sample. The pink regions represent GBs while the open space between boundaries is classified as GIs. A movie of this 3D segmentation map is provided in the Supporting Information. Additionally, a slice of this 3D classification map is also shown in the inset of Figure 3c. At the surface, this PL threshold closely matches with GB locations determined by EBSD (Figure 3c), confirming that the PL intensity can reliably discriminate between GBs and GIs.

By applying this classification over the entire 3D volume, we show in Figure 4b the median lifetimes of the GI (green) and GB (blue) areas as a function of depth below the surface for the as-deposited sample. General trends of the entire area

Adv. Mater. **2016**,
DOI: 10.1002/adma.201603801

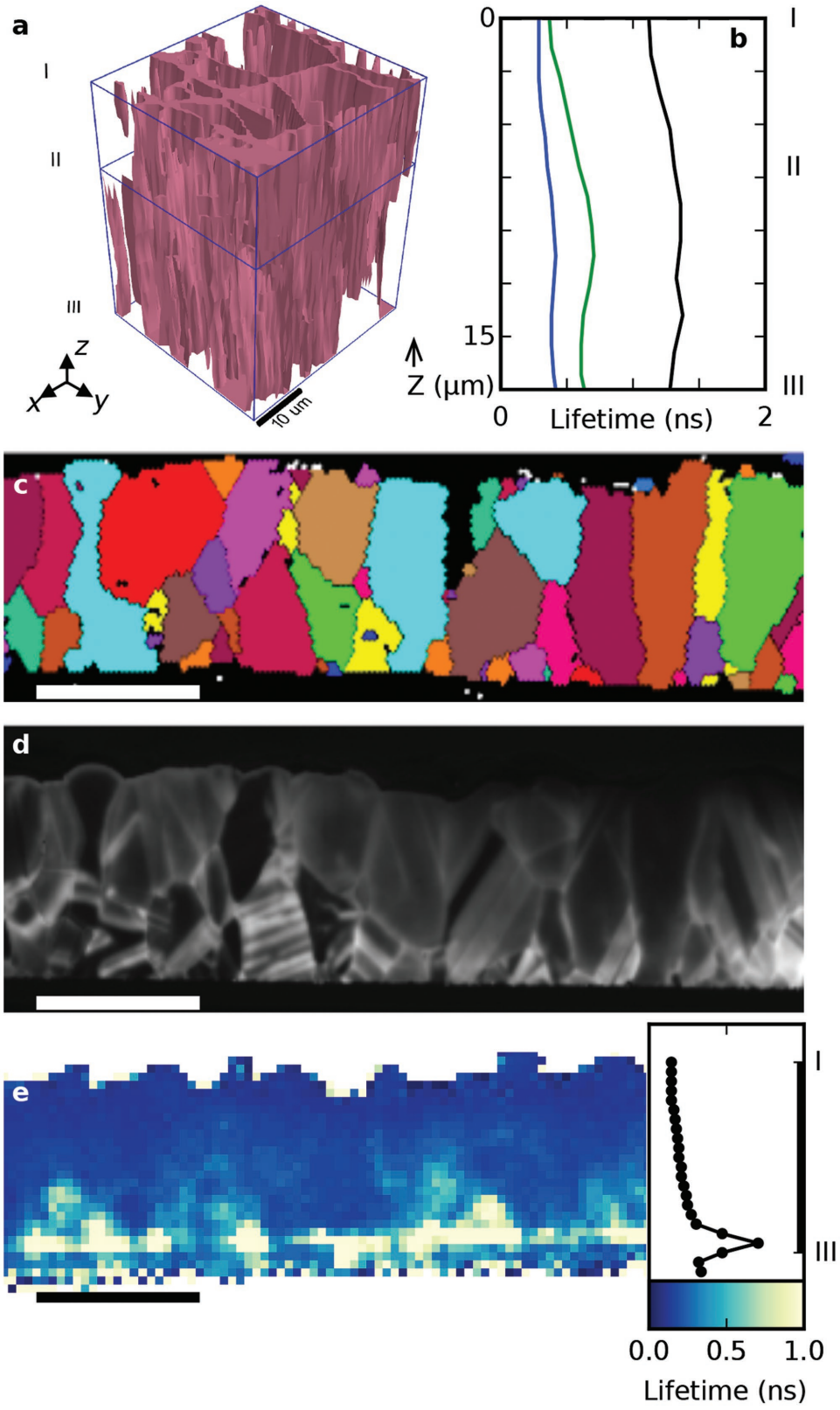

Figure 4. Depth analysis of carrier lifetimes in CdTe films and a cross-sectioned PV device. a) PL intensity threshold-based discrimination between voxels of GBs and GIs for the as-deposited sample. Pink areas are GB regions, while the open spaces between them are the GI volumes. Scale bar is 10 µm. b) Median carrier lifetime as a function of depth into the as-deposited sample in GB regions (blue), and GIs (green). Median carrier lifetime as a function of depth into the $CdCl_2$-treated sample is shown in black. c) EBSD map of grains of cross-sectioned PV device. d) EBIC map of the same cross-section. e) 2P lifetime map of the same cross-section. Inset shows median lifetime as a function of depth. c–e) Scale bars are 5 µm.

are: I) median lifetime is shortest at the CdTe sample surface, which is where the back contact of the cell would be placed; II) the lifetime increases toward the bulk, peaking at a depth of ≈5 µm beneath the top surface; and III) the lifetime then decreases near the CdTe/CdS junction where the CdTe growth is initiated. These trends apply to both GI and GB areas, but are more pronounced in the GIs. The GB lifetimes are uniformly smaller than the GI lifetimes throughout the depth of the film. At the exposed surface (I), short carrier lifetimes are typical of CdTe films (and other semiconductors) and arise mostly from surface-related defects caused by intrinsic surface states, atmospheric exposure, and mechanical processing such as polishing.[17,23] We note that lifetime measurements on unpolished samples also exhibit reduced surface lifetime compared to subsurface areas, demonstrating that a polishing treatment is not the sole source for increased surface recombination (see Figure 4e and Supporting Information).

Although discerning the changes in lifetime with probe depth for GB and GI regions is not possible for the treated sample, an average trend through the bulk is identifiable. We plot in black in Figure 4b the median lifetime for all voxels as a function of depth for this $CdCl_2$-treated sample. The lifetime is slightly reduced at the surface and the buried interface relative to the bulk of the film, but to a much smaller degree compared to the as-deposited sample. Unlike the as-deposited sample, the variation does not follow grain structure and the treatment significantly improved lifetimes at all depths compared to the as-deposited sample. Most interestingly, the treatment significantly increases lifetime at the buried CdTe/CdS interface (III) relative to the same region in the as-deposited sample's junction, indicating that the $CdCl_2$ treatment penetrates the entire 15-µm-thick film and significantly improve lifetimes in the critical junction region by a factor of 2. There is no appearance of GB like structures with reduced lifetime deeper in the film (see Figure 2d), which indicates that GBs appear to be largely passivated throughout the film.

Finally, we acquired 2P-TRPL maps from a completed CdTe PV device that has been cross-sectioned with a focused ion beam (FIB) and correlated them with EBSD and electron-beam-induced current (EBIC) maps. Figure 4c shows an EBSD map of a FIB cross-section of the 5-µm thick cross-sectioned solar cell. We observe in this EBSD map the columnar grain structure typical of CSS grown CdTe. A correlated EBIC map in Figure 4d shows that increased current is extracted close to GBs, in line with previous work.[9] The enhanced current at GBs can be attributed to either changes in electron beam carrier generation or band bending near GB defects and impurities that attracts electrons. Correlated 1P- and 2P-TRPL measurements are subsequently performed and 2P lifetime maps are plotted in Figure 4e. Notably, one-photon maps yield almost no contrast in lifetime as they are dominated by recombination from the surface of the cross-sectioned face (see Supporting Information). Meanwhile, 2P measurements penetrate beyond the surface, enabling us to observe lifetime variations throughout the cross-section. Unlike the EBIC measurements, GBs do not produce contrast in 2P lifetime maps within the resolution limitations of the measurement, indicating that the GB band bending is independent of carrier lifetime.

The 2P lifetime map in Figure 4e indicates the lifetime is lowest at the back-contact (I) and increases toward the CdTe/CdS junction (III), where lifetime is longest. This increase in lifetime at the p–n junction in treated devices elucidates a critical efficiency-enhancing mechanism, and is similar to the depth trends seen in the in situ 3D scans of the thicker (15 µm), treated CdTe film seen in Figure 4b. We also observe lateral variations in lifetime, but these variations do not correlate directly to grain structure from the EBSD measurements. We observe that some grains have different lifetimes than neighboring grains, but no lifetime shortening is observed at GBs, which is also in agreement with the GB results on thick samples. Interestingly we observe a large increase in lifetime near the CdTe/CdS junction. Sulfur diffusion during the $CdCl_2$ treatment can increase the lifetime near the CdTe/CdS interface[24] and may explain this strong lifetime increase. With the thicker (≈15 µm) samples we do not observe such a lifetime peak near the buried junction (Figure 2d and Figure 4b). It is plausible that the depth resolution when probing from the back-contact cannot resolve such sharp features, unlike our observations from the thin cross-sectioned sample.

We have measured spatially resolved 3D carrier-lifetime maps using 2P tomography to uncover carrier dynamics at buried structures in CdTe thin-films photovoltaics. Enhanced carrier recombination rates are commonly associated with increased nonradiative recombination pathways that are mediated by defects. When thin-film CdTe solar cells are initially deposited, we observe increased nonradiative carrier recombination at GBs throughout the 3D volume of the film, which is most pronounced in the critical junction region where small nucleation grains form at the buried CdTe/CdS interface. The data on CdTe films treated by exposure to $CdCl_2$ vapor reveal that a critical function of the treatment is to reduce surface, interface and GB recombination throughout the entirety of these polycrystalline films. The $CdCl_2$ treatment may also compensate CdTe films, making it difficult to exceed a hole density of 10^{15} cm^{-3} and achieve higher V_{oc} and efficiency. This work indicates that removing the $CdCl_2$ treatment would require shifting to larger grain materials, and/or finding alternative methods to passivate the surface, interfaces, and grain boundaries.

By peering below the surface of a sample, we can avoid mistaking surface effects as intrinsic properties of a film. For example, in CdTe photovoltaics Cu insertion can decrease lifetime preferentially at the back contact yet increase hole density. By using this multiphoton technique to penetrate a focused excitation volume well into the bulk, interference from such surface-related processes is minimized and the measured properties better reflect the intrinsic bulk properties. This is a critical and unmatched advantage of this technique, as it allows in situ characterization of bulk properties without the need for elaborate surface passivation that is otherwise irrelevant to the fabrication process of a functional device. This technique can be applied to a host of materials including lead–halide perovskites, CdSe, $Cu(In,Ga)Se_2$, GaN, and copper zinc tin sulfide (CZTS) to provide scientific understanding of surface, interface, grain-boundary, and bulk recombination dynamics throughout polycrystalline and inhomogeneous materials for electro-optical and other applications.

Adv. Mater. 2016,
DOI: 10.1002/adma.201603801

Supporting Information

Supporting Information is available from the Wiley Online Library or from the author.

Acknowledgements

This work was partially performed at the Molecular Foundry, Lawrence Berkeley National Laboratory, and was supported by the Office of Science, Office of Basic Energy Sciences, Scientific User Facilities Division, of the U.S. Department of Energy (DOE) under Contract No. DE-AC02-05CH11231. The work at the National Renewable Energy Laboratory was supported by the DOE, Office of Energy Efficiency and Renewable Energy (EERE), under Contract No. DE-AC36-08GO28308. This material is based upon work supported by the DOE under Award Number DE-EE0005953. ESB was supported by a DOE EERE SunShot Postdoctoral Research Award.

Received: July 18, 2016
Revised: September 15, 2016
Published online:

[1] National Renewable Energy Laboratory, "Best Research-Cell Efficiencies," http://www.nrel.gov/ncpv/images/efficiency_chart.jpg, accessed: June 2016.
[2] First Solar, Inc., "First Solar Utility Scale Generation," http://www.firstsolar.com/solutions/utility-scale-generation, accessed: June 2016.
[3] M. Terheggen, H. Heinrich, G. Kostorz, D. Baetzner, A. Romeo, A. N. Tiwari, *Interface Sci.* **2004**, *12*, 259.
[4] J. M. Burst, J. N. Duenow, D. S. Albin, E. Colegrove, M. O. Reese, J. A. Aguiar, C.-S. Jiang, M. K. Patel, M. M. Al-Jassim, D. Kuciauskas, S. Swain, T. Ablekim, K. G. Lynn, W. K. Metzger, *Nat. Energy* **2016**, *1*, 16015.
[5] B. M. Başol, *Int. J. Sol. Energy* **1992**, *12*, 25.
[6] I. Dharmadasa, *Coatings* **2014**, *4*, 282.
[7] B. E. McCandless, L. V. Moulton, R. W. Birkmire, *Prog. Photovoltaics Res. Appl.* **1997**, *5*, 249.
[8] H. R. Moutinho, M. M. Al-Jassim, F. A. Abulfotuh, D. H. Levi, P. C. Dippo, R. G. Dhere, L. L. Kazmerski, in *Conference Record of the Twenty-Sixth IEEE Photovoltaic Specialists Conference, 1997*, IEEE, Piscataway, NJ, USA, **1997**, pp. 431–434, DOI: 10.1109/PVSC.1997.654120.
[9] C. Li, Y. Wu, J. Poplawsky, T. J. Pennycook, N. Paudel, W. Yin, S. J. Haigh, M. P. Oxley, A. R. Lupini, M. Al-Jassim, S. J. Pennycook, Y. Yan, *Phys. Rev. Lett.* **2014**, *112*, 156103.
[10] J. Moseley, M. M. Al-Jassim, D. Kuciauskas, H. R. Moutinho, N. Paudel, H. L. Guthrey, Y. Yan, W. K. Metzger, R. K. Ahrenkiel, *IEEE J. Photovoltaics* **2014**, *4*, 1671.
[11] J. Moseley, W. K. Metzger, H. R. Moutinho, N. Paudel, H. L. Guthrey, Y. Yan, R. K. Ahrenkiel, M. M. Al-Jassim, *J. Appl. Phys.* **2015**, *118*, 25702.
[12] A. Kanevce, J. Moseley, M. Al-Jassim, W. K. Metzger, *IEEE J. Photovoltaics* **2015**, *5*, 1722.
[13] K. Durose, D. Boyle, A. Abken, C. J. Ottley, P. Nollet, S. Degrave, M. Burgelman, R. Wendt, J. Beier, D. Bonnet, *Phys. Status Solidi B* **2002**, *229*, 1055.
[14] I. Visoly-Fisher, S. R. Cohen, K. Gartsman, A. Ruzin, D. Cahen, *Adv. Funct. Mater.* **2006**, *16*, 649.
[15] W. K. Metzger, M. Gloeckler, *J. Appl. Phys.* **2005**, *98*, 63701.
[16] D. W. de Quilettes, S. M. Vorpahl, S. D. Stranks, H. Nagaoka, G. E. Eperon, M. E. Ziffer, H. J. Snaith, D. S. Ginger, *Science* **2015**, *348*, 683.
[17] E. S. Barnard, E. T. Hoke, S. T. Connor, J. R. Groves, T. Kuykendall, Z. Yan, E. C. Samulon, E. D. Bourret-Courchesne, S. Aloni, P. J. Schuck, C. H. Peters, B. E. Hardin, *Sci. Rep.* **2013**, *3*, 2098.
[18] F. Helmchen, W. Denk, *Nat. Methods* **2005**, *2*, 932.
[19] J. Ma, D. Kuciauskas, D. Albin, R. Bhattacharya, M. Reese, T. Barnes, J. V. Li, T. Gessert, S.-H. Wei, *Phys. Rev. Lett.* **2013**, *111*, 67402.
[20] D. Kuciauskas, S. Farrell, P. Dippo, J. Moseley, H. Moutinho, J. V. Li, A. M. A. Motz, A. Kanevce, K. Zaunbrecher, T. A. Gessert, D. H. Levi, W. K. Metzger, E. Colegrove, S. Sivananthan, *J. Appl. Phys.* **2014**, *116*, 123108.
[21] P. J. Schuck, R. D. Grober, A. M. Roskowski, S. Einfeldt, R. F. Davis, *Appl. Phys. Lett.* **2002**, *81*, 1984.
[22] W. K. Metzger, R. K. Ahrenkiel, J. Dashdorj, D. J. Friedman, *Phys. Rev. B* **2005**, *71*, 035301.
[23] J. Luschitz, K. Lakus-Wollny, A. Klein, W. Jaegermann, *Thin Solid Films* **2007**, *515*, 5814.
[24] W. K. Metzger, D. Albin, M. J. Romero, P. Dippo, M. Young, *J. Appl. Phys.* **2006**, *99*, 103703.